Results in Physics 14 (2019) 102380

Contents lists available at ScienceDirect

Results in Physics

journal homepage: www.elsevier.com/locate/rinp

Synthesis and electrochemical properties of polyaniline/$Co(OH)_2$–$Ni(OH)_2$ nanocomposite electrode materials

Janardhan H. Shendkar[a,b], Vijaykumar V. Jadhav[c,e,*], Pritamkumar V. Shinde[d], Rajaram S. Mane[b,*]

[a] S. S. J. E S. Arts, Comm. and Sci. College, Gangakhed, Dist. Parbhani, India
[b] School of Physical Sciences, Swami Ramanand Teerth Marathwada University, Nanded, India
[c] Department of Physics, Shivaji Mahavidyalaya, Udgir, Dist. Latur, MH, India
[d] Global Frontier R&D Center for Hybrid Interface Materials, Pusan National University, Busan, South Korea
[e] Guangdong Technion-Israel Institute of Technology, Shantou, Guangdong Province, China

ARTICLE INFO

Keywords:
Electrochemical supercapacitor
Electrochemical deposition
Polyaniline
Nanofibers
Nanoplatelets
Nanocomposites

ABSTRACT

Electrochemical supercapacitive properties of polyaniline (PANI)/cobalt hydroxide ($Co(OH)_2$)–nickel hydroxide ($Ni(OH)_2$) nanocomposite (NC) electrode materials, synthesized potentiostatically *via* a electrochemical deposition method, are explored and compared with PANI and $Co(OH)_2$–$Ni(OH)_2$ electrode materials. From the surface analysis, an amorphous PANI, NCs and $Co(OH)_2$–$Ni(OH)_2$ are entirely different from one another. The PANI surface demonstrates nanofibrous morphology, NCs exhibits nanofiber-platelet morphology and Co $(OH)_2$–$Ni(OH)_2$ endows platelet-type surface morphology. The electrochemical properties of the PANI, NCs and $Co(OH)_2$–$Ni(OH)_2$ electrode materials are obtained from the cyclic-voltammetry and galvanostatic charge-discharge measurements. The specific capacitances of PANI, NCs and $Co(OH)_2$–$Ni(OH)_2$ measured at a sweep rate of 10 mV/s in a 1.0 M NaOH electrolyte are found to be 0.59, 50.0–74.1 and 312.5 F/g, respectively. The retention values of PANI, NCs and $Co(OH)_2$–$Ni(OH)_2$ obtained at the same scan rate for 1000 cycles are 25.8, 70.5–57 and 42.4%, respectively. This work clearly illustrates the reasons for a weak electrochemical performance of PANI and its composites with $Co(OH)_2$–$Ni(OH)_2$ in alkaline electrolyte over $Co(OH)_2$–$Ni(OH)_2$ electrode material.

Introduction

The development of global economy, the increasing demand of energy which depleted the fossil fuel and increased environmental pollution, has created the need for clean, efficient and sustainable energy sources. These clean, reliable and sustainable energy sources are supposed to have the technological applications. Hence, energy storage devices like batteries, capacitors and supercapacitors have received a prime importance nowadays. From several energy storage devices electrochemical supercapacitors, as a source of high power density, are essentially used in hybrid electric vehicles and portable electronic items [1]. Therefore, the protection against power disruption of batteries or fuel cells can overcome by providing complimentary back up power through supercapacitors, and moreover, they minimise the energy density and power density gap between conventional capacitors and batteries [2,3]. Depending upon the charge storage mechanism electric double layer capacitors, where charges store at interface of electrode/electrolyte electrostatically, and pseudocapacitors or redox or faradaic supercapacitors where charges store by a virue ofredox reactions between electrode material and electrolyte are two forms of supercapacitors [4]. The main problem in the development of supercapacitor technology is its low energy density which can be cover up by adding a material of high battery-type material as a composite material. It has been evidenced that the limitations of carbon/polymer-based supercapacitor materials are defeated by adding either battery or pseudocapacitor-type electrode materials. The supercapacitive materials like carbon, conducting polymers, metal oxides/hydroxides and their composites [4–6] have received considerable attention in synergistic electrode materials. The specific capacitance (SC) of carbon-based electrode materials is caused by electric double layer capacitance kinetics, which mainly depends upon the surface area accessibility and electrical conductivity. The porous nature of carbon provides a high surface area and hence, a low SC which directed scientists to look after the composite electrode materials i.e. addition of conducting polymer in transition metal oxides/hydroxides etc. [7]. The conducting polymers/oxides/hydroxides/layered double hydroxides etc., have demonstrated a

* Corresponding authors at: Department of Physics, Shivaji Mahavidyalaya, Udgir, Dist. Latur, MH, India (V.V. Jadhav).
E-mail addresses: vijaykumar.jadhav@gtiit.edu.cn (V.V. Jadhav), rajarammane70@srtmun.ac.in (R.S. Mane).

https://doi.org/10.1016/j.rinp.2019.102380
Received 23 April 2019; Received in revised form 22 May 2019; Accepted 22 May 2019
Available online 25 May 2019

pseudocapacitance nature due to their intercalation/de-intercalation kinetics. Polyaniline, one of the most important conducting polymers, is suffering from a low cycling life [8] and metal oxides/hydroxides like RuO_2, $MnO_2/Mn(OH)_2$, $CoO/Co_2O_3/Co(OH)_2$, $NiO/Ni(OH)_2$ demonstrated commercial cavalry due issue caused by dissociation/corrosion in spite of their high performance on account of several redox reactions [3].

Instead of noble transition metal oxides/hydroxide more attention has been paid on utilizing cheaper transition metal oxides/hydroxides like MnO_2, $[M^{2+}_{1-x}, M^{3+}_{x}\ (OH)_2]^{x+}\ (A^{n-1})_{n/2}{\cdot}mH_2O$, $MnCO_3$, $CoO/Co_2O_3/Co(OH)_2$ and $NiO/Ni(OH)_2$ etc., in supercapacitor technology. The preference of cobalt and nickel oxides/hydroxides lies not only due to their cheaper cost, but also due to their availability in several well-defined redox states, easyness with which they synthesized and high theoretical supercapacitance value [9]. Nickel hydroxide ($Ni(OH)_2$) reveals a low electrical conductivity [10] and weak adhesive force of attraction between current collecting substrate and nickel-based materials [11] due to which its rate capability, reversibility and hence cycle stability is hampered to some extent. The above problems can be solved by; i) depositing $Ni(OH)_2$ directly onto a three dimensional nickel foam (Ni-foam) for high specific capacitance [12] due to addition of capacitance of Ni-foam and less mass deposition, ii) intercalating anions like Cl^-, NO_3^- and SO_4^{2-} in $Ni(OH)_2$ to exhibit enhancement in SC [13], iii) refining electrode materials with nanosheets morphology also enhances the SC [14], iv) making composite of $Ni(OH)_2$ with other transition metal oxides/hydroxides [15–19], v) developing the composites with conducting reduced graphene oxides with enhanced specific capacitance and increased cycle life [20,21], vi) doping Mn [22] like metals of several redox states. It is to be noted that these polymers are stable in acidic electrolytes whereas, metal oxides are in an alkaline electrolytes. The non-usability of polymers in alkaline electrolyte has rarely been addressed thereby, this study explores in-depth investigation on the use of polymer/metal hydroxide composite (NC) electrode materials in electrochemical supercapacitor (ES) applications.

Composite electrodes of polyaniline/cobalt hydroxide–nickel hydroxide (PANI/$Co(OH)_2$–$Ni(OH)_2$) were synthesized onto a stainless-less steel (SS) substrate and, after physical measurements i.e. X-ray diffraction (XRD), field emission scanning electron microscope (FESEM), energy dispersive X-ray (EDX), they were envisaged for their electrochemical properties like cyclic voltammetry (CV) and galvanostatic charge – discharge (GCD).

Experimental section

Materials

All chemical reagents were analytical grade, purchased from Merck and used without further purification. The chemicals used were cobalt nitrate [$Co(OH)_2{\cdot}6H_2O$], nickel nitrate [$Ni(OH)_2{\cdot}6H_2O$], sodium hydroxide [NaOH], and acetone. The aqueous solutions were prepared in double distilled water.

Preparation of PANI

The polymerization of 0.5 M aniline was carried out in standard three-electrode glass cell potentiostatically onto a SS working electrode of 1 cm^2 area at 0.75 V for 5 min deposition time in the presence of platinum plate as a counter electrode and Ag/AgCl as a reference electrode. The precursor for polymerization was a homogenous mixed solution of 0.5 M aniline monomer and 0.5 M sulphuric acid, adjusted to a pH < 2. The SS substrate of 1 cm^2 was polished with a zero-polishing paper, ultrasonically cleaned in distilled water and acetone, and then dried in air before electrodeposition process and referred as (C1) electrode in the present study.

Preparation of NCs, and $Co(OH)_2$–$Ni(OH)_2$ electrodes

The composite (PANI/$Co(OH)_2$–$Ni(OH)_2$)) electrode materials were prepared in three-electrode glass cell at a constant potential of −1.0 V for 5 min and named as (C2), 10 min (C3), 15 min (C4) and 20 min (C5) over PANI surface. The precursor solution for electrodeposition was a mixture of 0.05 M cobalt nitrate and 0.05 M nickel nitrate. The prepared composite electrodes were again immersed into the distilled water and dried in air before their final use. The cathodic electrodeposition was applied for obtaining $Co(OH)_2$–$Ni(OH)_2$ electrodes at constant potential of −1.0 V for 10 min and named as (C6). The mass of active electrode material loaded onto a SS substrate was determined on comparing the difference between the SS and PANI, NCs and Co $(OH)_2$–$Ni(OH)_2$ which were 1.9, 2.4, 2.6, 2.8, 2.95 and 2.66 mg/cm^2 for (C1) to (C6) electrode materials, respectively. The difference in the masses of deposited electrode materials was not surprisingly high.

Characterizations

The crystal structures of PANI, NCs and $Co(OH)_2$–$Ni(OH)_2$ electrode materials were confirmed from XRD patterns, recorded on D8-Discovery Bruker X-ray diffractometer which was operated under 40 kV, 40 mA, and Cu Kα, λ = 1.5406 Å operating conditions in θ-2θ geometry. The surface morphologies and qualitative elemental analysis measurements of (C1)-(C6) electrode materials were confirmed by a field-emission scanning electron microscopy (FESEM) images, recorded on Hitachi S-4800 at 15 kV accelerating voltage equipped with energy dispersive X-ray spectroscopy (EDX). Electrochemical measurements such as CV and GCD were performed on electrochemical work station WonAtech. The galvanostatic charging-discharging measurements were attempted on IVIUMSTAT workstation, the Netherlands. The electrochemical measurements were studied at room-temperature (27 °C) in a 1.0 M NaOH aqueous electrolyte solution.

Results and discussion

Reaction kinetics

The anodic electrodeposition of PANI was carried out potentiostatically at 0.75 V as above this potential non-conducting pernigraniline state of PANI is favoured instead of forming conducting emeraldine PANI [23]. The applied potential resulted in the formation of 2D thin compact layer/film of PANI onto a SS substrate. Then an increased continuous consumption of aniline monomer in electrodeposition limits the formation of new nuclei which changes the surface morphology from 2D plates to 1D nanofibers [24]. The electrodeposition of the Co $(OH)_2$ and $Ni(OH)_2$ onto a SS-PANI and SS was a result of nitrate ions reduction, which increases the local pH of the solution close to the cathode by forming OH^- ions. The reaction of the OH^- ions with Co^{2+} and Ni^{2+} ions from electrolyte solution results the deposition of Co $(OH)_2$–$Ni(OH)_2$ deposits onto PANI-SS and SS electrodes could be as follows [25,26]

$$NO_3^- + 7H_2O + 8e^- \rightarrow NH_4^+ + 10OH^- \quad (1)$$

$$Co^{2+} + 2OH^- \rightarrow Co(OH)_2 \quad (2)$$

$$Ni^{2+} + 2OH^- \rightarrow Ni(OH)_2 \quad (3)$$

Structural elucidation

The structures of PANI, NCs and $Co(OH)_2$–$Ni(OH)_2$ (hereafter C1, C2, C3, C4, C5 and C6) electrodes were determined by the XRD patterns (Fig. 1). In the XRD pattern, the peaks marked with * symbol were of SS substrate. No new peaks were noted in all XRD patterns, suggesting the formation of an amorphous or nanocrystalline electrode materials.

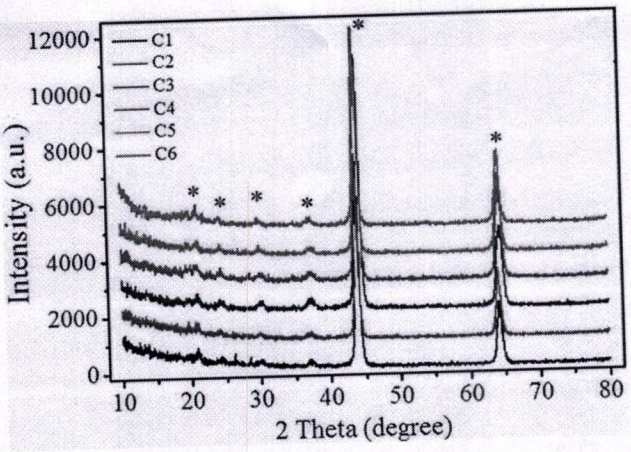

Fig. 1. The XRD spectra of C1–C6 electrodes.

Generally, polymers and metals hydroxides, obtained using soft chemical solution methods, are an amorphous in nature.

Elemental analysis

The EDX spectra are of C1–C6 electrodes are shown in Fig. 2. The EDX spectrum of C1 confirmed elements like carbon (C), nitrogen (N) of PANI and oxygen for absorbed water in PANI nanofiber network. In the EDX spectrums of C2–C5, basic elements were carbon (C), nitrogen (N), oxygen (O), cobalt (Co) and nickel (Ni). And in spectrum C6, elements like cobalt, nickel and oxygen were anticipated from $Co(OH)_2$ and $Ni(OH)_2$. The presence of iron (Fe) could be from the SS and the element platinum (Pt) is due to sputtering of very thin layer of platinum as all electrode materials were nonconductive in nature, which, in fact, is unprecedented. It is to be noted that in all EDX measurements only elementals like C, O, Ni and Co detected, confirming a qualitative analysis of the product materials.

Morphological evolution

The FESEM images of C1–C6 electrode materials are shown in Fig. 3 where, a nanofibrous surface morphology of C1 with diameters ranging from 50 to 100 nm is evidenced. The open spaces present in-between them could provide direct paths for the ions of electrolyte to access a maximum electrode material surface for better performance. The FESEM images of C2–C5 are the surfaces of NC electrodes. With increase of time, the electrodeposition of $Co(OH)_2$ and $Ni(OH)_2$ onto PANI nanofibers increases by connecting these nanofibers (Fig. 3C2, C3). But, in the FESEM images of C4 & C5, the deposition was not well clear as like in C2 & C3, though the specific capacitance of C4 was higher in all composite electrode materials, suggesting non-uniform deposition of $Co(OH)_2$ & $Ni(OH)_2$ over PANI nanofibers, as observed from respective FESEM images i.e. C2–C5 of Fig. 3. The FESEM image of C6 exhibited 2D platelet-type surface morphology of 20 to 30 nm in thickness.

CV measurement

The electrochemical capacitive properties of C1–C6 electrode materials were measured with CV spectra at the scan rate of 10 mV/s in 1.0 M NaOH aqueous electrolyte as shown in Fig. 4a. The mass loading and geometrical area of all active electrode materials were nearly same within potential range of −0.2 to 0.5 V for C1, 0.0 to 0.5 V for C2–C5 and −0.1 to 0.5 V for C6. An inset of Fig. 4a is an enlarged view of CV of C1 i.e. PANI, where instead of pronounced peak, increase in current

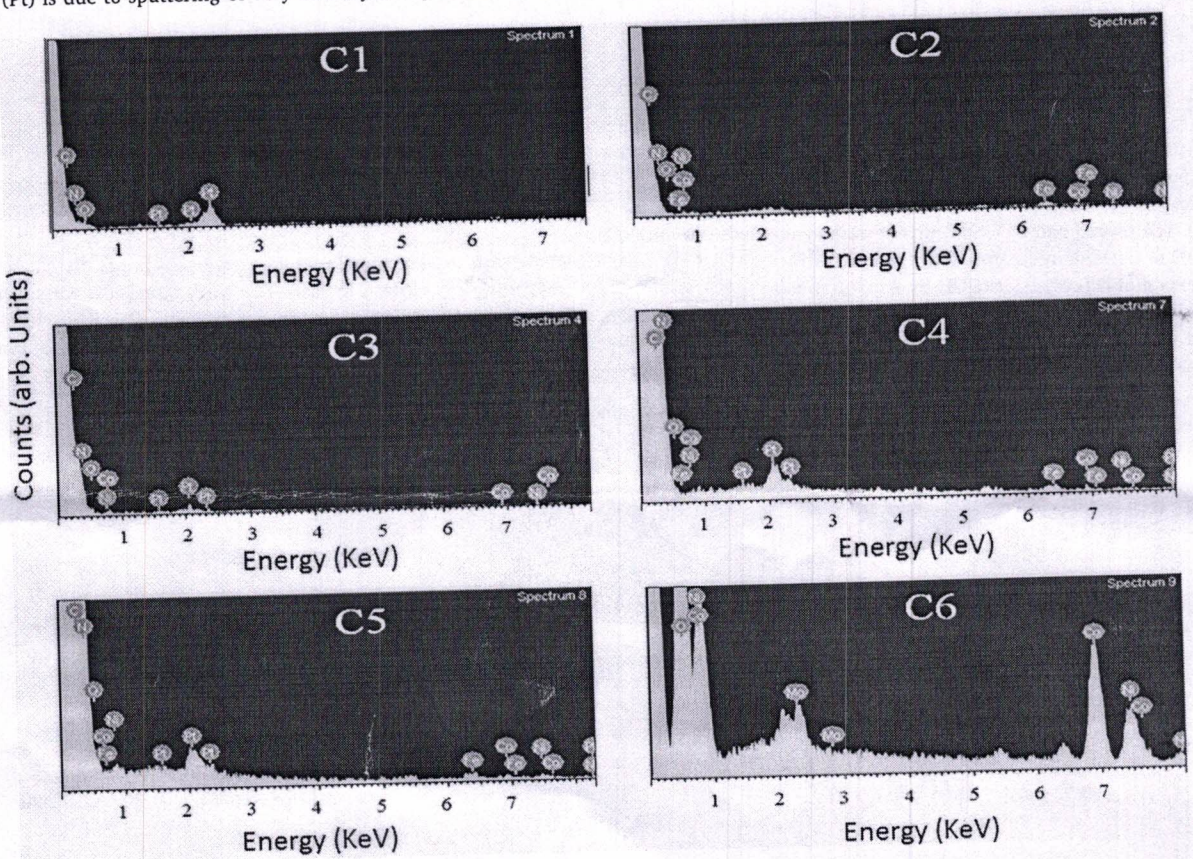

Fig. 2. The EDX spectrums showing elementals present over C1–C6 electrode surfaces.

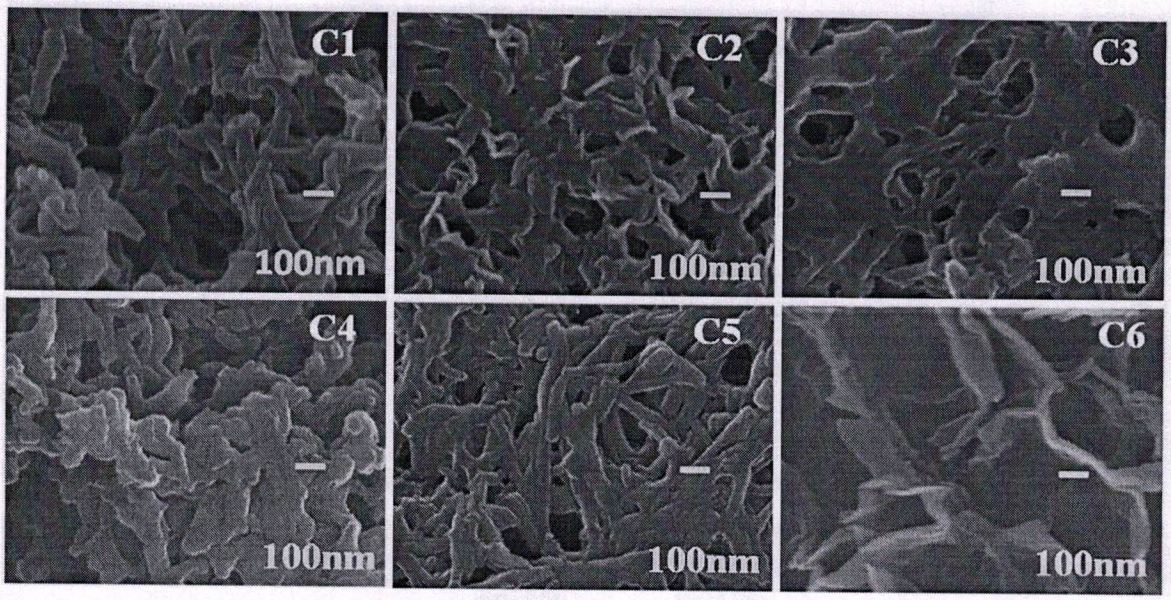

Fig. 3. The FESEM images of C1–C6 electrodes showing a surface change from nanorods to nanoplatelets.

with voltage (and decrease in current with decrease of voltage) is free from the redox activity in alkaline medium, hence the capacitance may be due to electrostatic adsorption and desorption of electrolyte ions at the surface of the electrode materials. While in NCs electrode materials i.e. C2–C5 as well as in C6 anodic and cathodic peaks are clearly seen on account of the presence of following redox reactions over $Co(OH)_2$ & $Ni(OH)_2$ [27,28]

$$Co(OH)_2 + OH^- \leftrightarrow CoOOH + H_2O + e^- \quad (4)$$

$$CoOOH + OH^- \leftrightarrow CoO + H_2O + e^- \quad (5)$$

$$Ni(OH)_2 + OH^- \leftrightarrow NiOOH + H_2O + e^- \quad (6)$$

The redox reactions of $Co(OH)_2$ involve $2e^-$ per redox reaction while $Ni(OH)_2$ involves $1e^-$ per redox reaction. The first pair of redox current peak of $Co(OH)_2$ is due to oxidation reaction conversion between $Co(OH)_2$ to CoOOH and reduction reaction in reverse direction (Eq. (4)). The second pair of redox current peak is due to the oxidation of CoOOH to CoO and reduction in the reverse direction (Eq. (5)). Due to conversion of $Ni(OH)_2$ to NiOOH by oxidation and in reverse direction by reduction for $Ni(OH)_2$ only one pair of redox current peak is obtained (Eq. (6)). The ideal shape of the CV of supercapacitive electrode material is rectangular. The CV curves of EDLC are more rectangular than that contain the redox reactions i.e. pseudocapacitive [29]. In the present case, the as-prepared C2–C5 electrodes demonstrated more rectangular shape as compared to C6. The area of CV, charge density, SC, energy density (E) and power density (P) of all electrode materials were determined by the following equations

$$A = \int I(V)\mathrm{d}V \quad (7)$$

$$q = \frac{1}{v}\int I(V)dV \quad (8)$$

$$SC = \frac{q}{m\nabla V} \quad (9)$$

$$E = \frac{1}{2}C_s(\nabla V)^2 \quad (10)$$

$$P = \frac{1}{2}C_s(\nabla V)\frac{dV}{dt} \quad (11)$$

where, A is area of the closed CV curve (mW), q is the charge density (mC/cm^2), $v = dV/dt$ is the scan rate (mV/s), m is the mass of electrode materials (g), ∇V is the potential window of CV, E is energy density (Wh/kg) and P is power density (W/kg). The maximum specific capacitance values obtained at 10 mV/s were 0.59, 50, 46.4, 85.7, 74.1 and

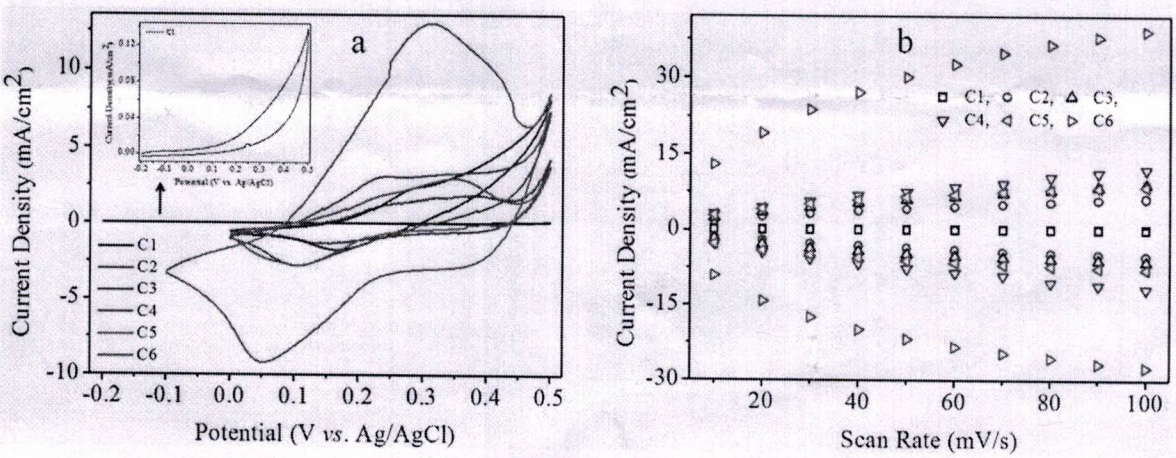

Fig. 4. (a) CV, and (b) scan rate *vs.* current density plots of C1–C6 electrodes.

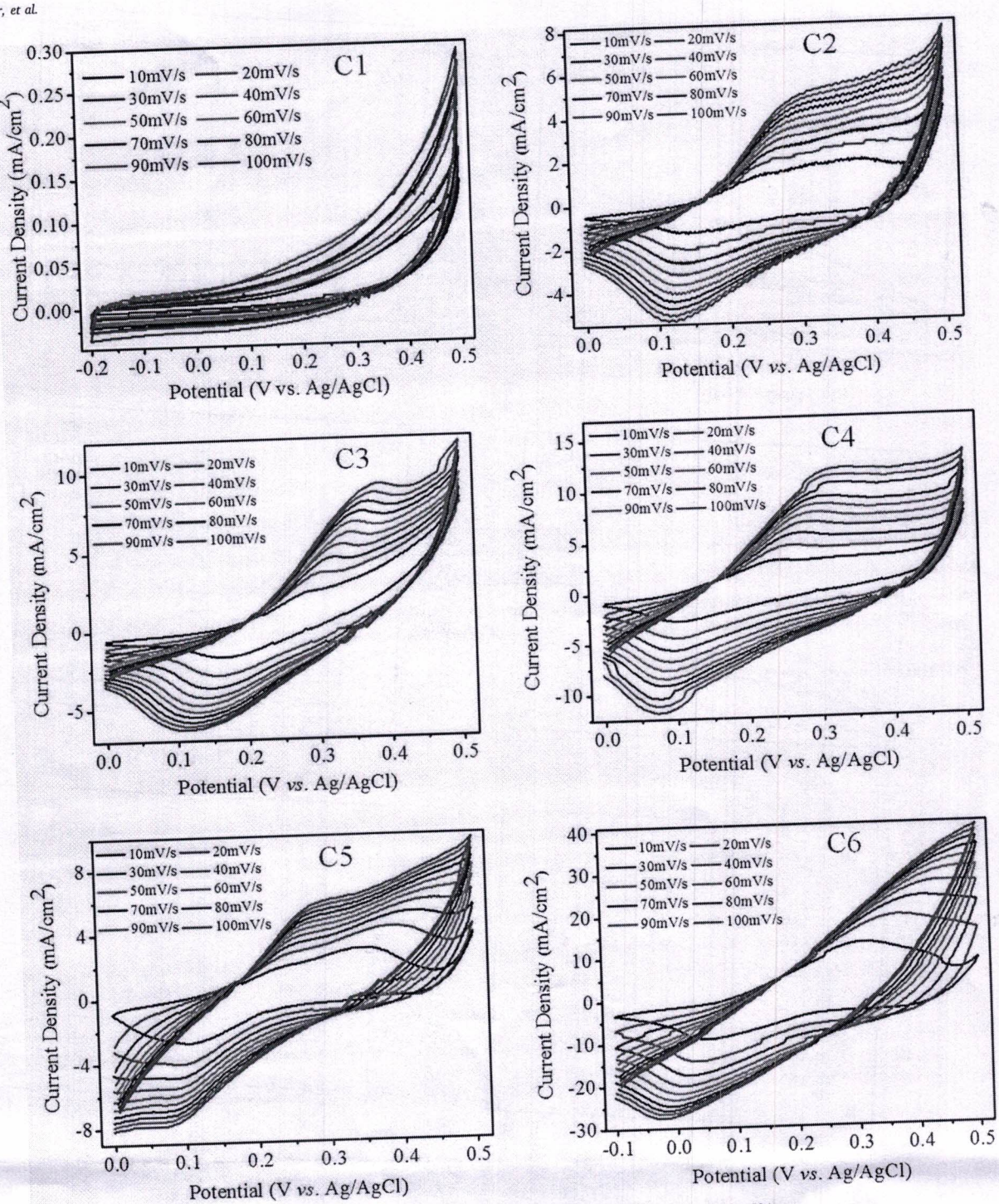

Fig. 5. The CV curves of C1–C6 electrodes at scan rate from 10 to 100 mV/s.

312.5 F/g for C1, C2, C3, C4, C5 and C6 electrode materials, respectively. The change in the performance is attributed to different; a) surface appearance, and b) charge transfer resistance. Among all electrode materials C6 revealed a high SC performance of 312.5 F/g over others, suggesting performance of PANNi and NCs electrode materials in alkaline electrolyte is inferior. The sweep rate effect on the performance of each electrode was carried out from 10 to 100 mV s^{-1} which is shown in Fig. 4b where, a linear relation is evidenced. The peak current (+ve/−ve) and area under each CV increased with the scan rate, evidencing a direct proportion relation between the area and the scan rate. The shape of CV is changed significantly from 10 to 100 mV/s for electrodes (Fig. 5C1–C6). The anodic current peaks moved towards the positive potential side, while cathodic current peaks towards the negative potential side, which is a function of availability of electrode material. In present case, the anodic/cathodic current density increases with scan rate, but is failed to maintain a linear relation with scan rate, suggesting the current density produced by active sites of electrode materials is not only surface dependent but is diffusion dependent also [30]. The deviation of the current density from a linear variation with scan rate is more for C6 than other electrode materials. But, for C4

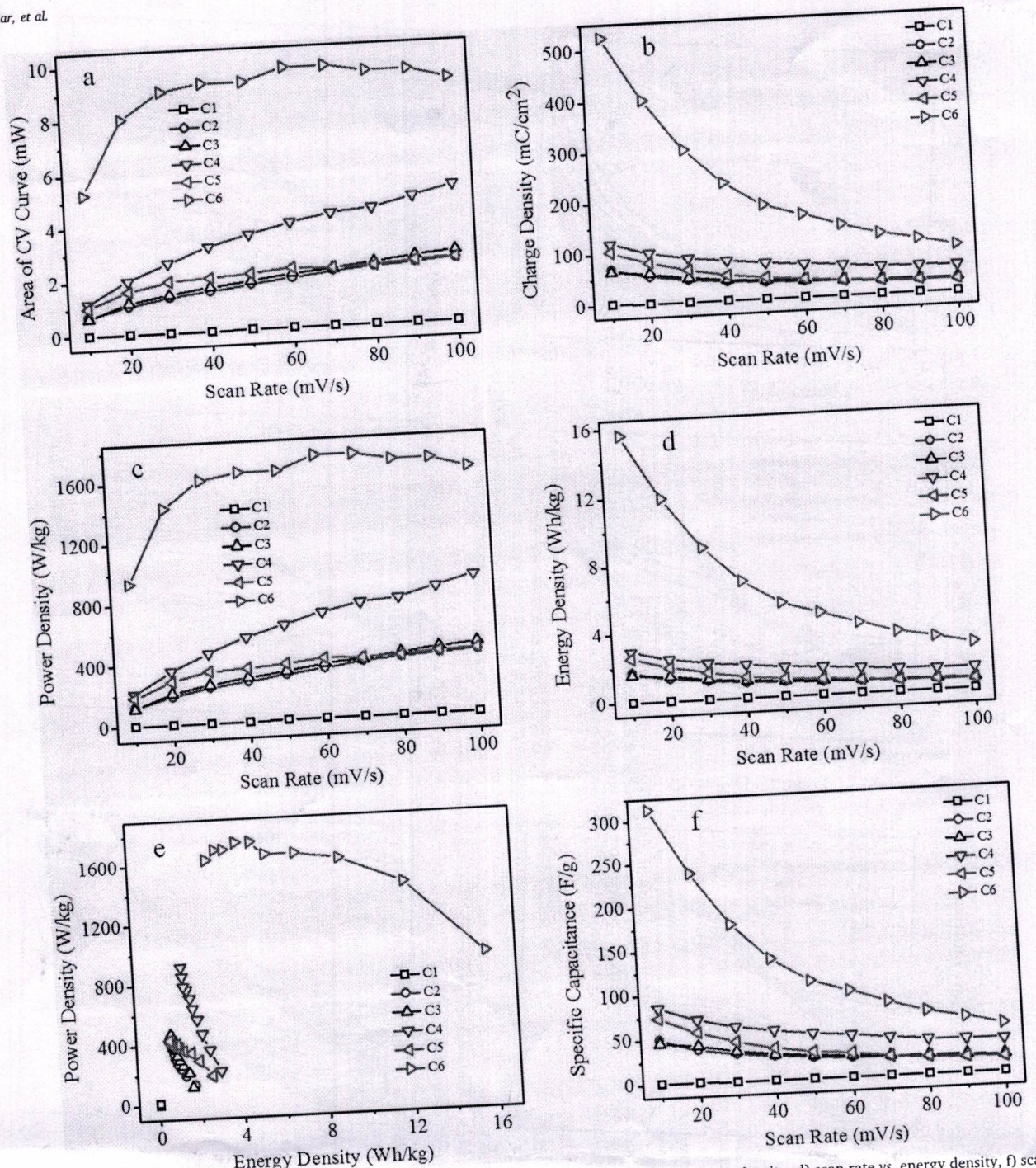

Fig. 6. The plots of; a) scan rate *vs.* area of the CV curve, b) scan rate *vs.* charge density, c) scan rate *vs.* power density, d) scan rate *vs.* energy density, f) scan rate *vs.* specific capacitance, and e) energy density *vs.* power density of the C1–C6 electrodes.

electrode the variation of current density is approximately more linear with scan rate.

Scan rate effect

The scan rate relation with area of CV curve, charge density, power density and energy density are shown in Fig. 6 (a-d) confirming more or less a similar nature. The area of CV curve should linearly vary with scan rate for good response. From Fig. 6a it is observed that the area under CV curve for C6 electrode increased with scan rate initially and then, approximately, remained unchanged, suggesting its more usefulness at lower scan rates and not at higher scan rates. But, in case of electrode C4, the area under CV curve increases with of scan rate, showing its better performance over NCs and C6 electrode materials. The percentage retentions (%) of CV curves, as a function of scan rate, with charge, power and energy densities confirmed a better contribution of C6 over C1 and rest electrode materials. The same nature of retention for charge density, specific capacitance and energy density values was evidenced. The power density *vs.* energy plots of C1–C6 electrode materials endowed better performance of C6 that of others. From the scan rate effect study one can approve a better performance of C6 electrode than PANI and NCs electrodes. The plot between energy

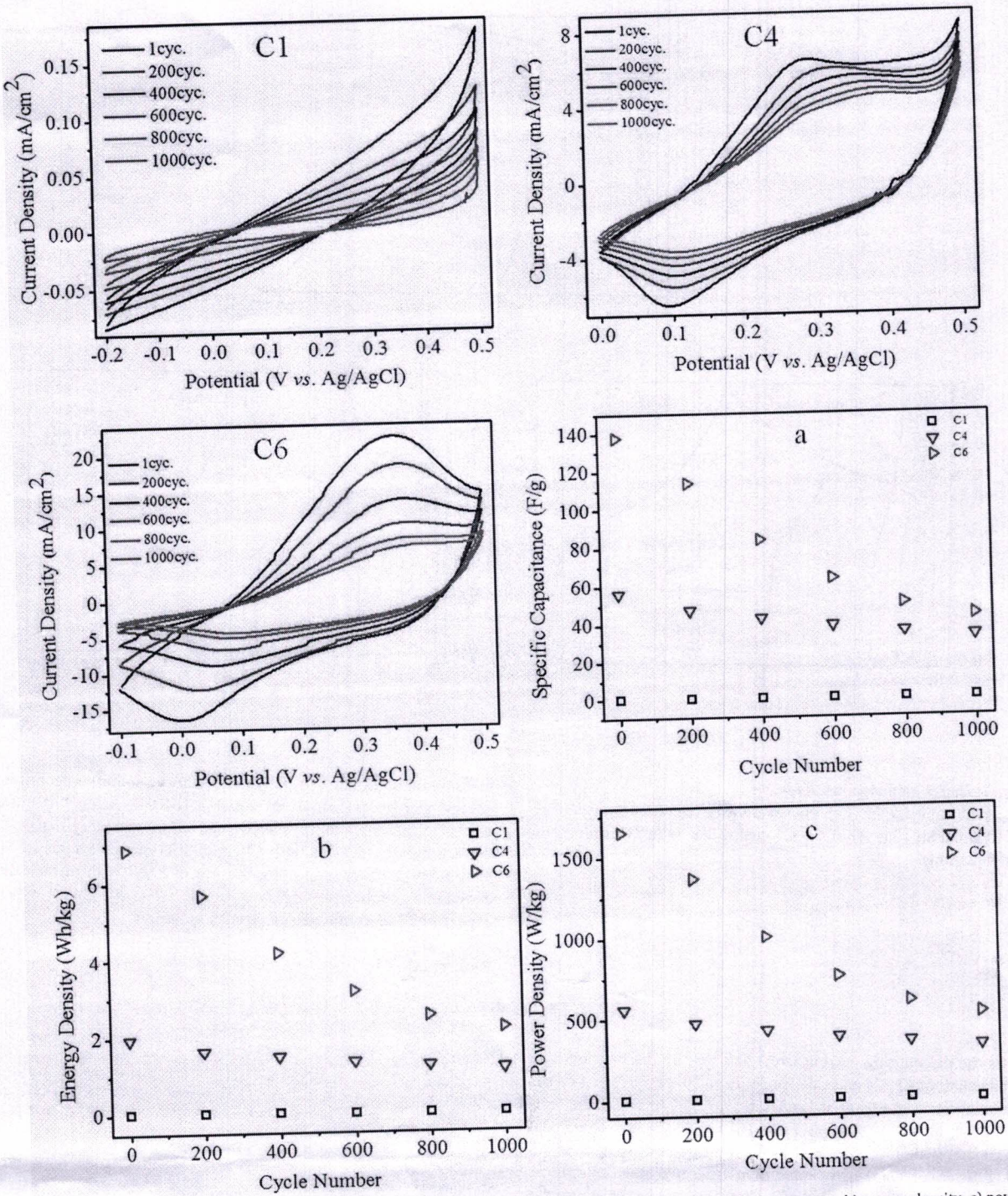

Fig. 7. CV plots of C1, C4 and C6 electrode materials from 1st to 1000th cycles. Plots of cycle number *vs.*; a-c) specific capacitance, b) energy density, c) power density of C1, C4 & C6 electrodes.

density and power density as shown in Fig. 6e suggested a better response for C6 electrode, so electrochemical stability properties of three electrodes i.e. C1, C4 and C6 were studied in rest of the work. Effect of specific capacitance *vs.* scan rate of all electrode materials as provided in Fig. 6f for C1–C6 electrodes at all scan rates corroborated a better performance of C6 electrode over others which may be due to a small charge resistance and availability of several redox states.

Cycling stability

The cycling tests of C1, C4 and C6 electrodes were operated for 1000 cycles to find the effect of cycling number on the specific capacitance, energy density and power density (Fig. 7C1, C4 and C6). From the cyclic stability curves it is inferred that the C6 electrode material availed higher specific capacitance, energy density and power density over C1 and C4 electrodes (Fig. 7a-c), suggesting presence of better adhesion force of attraction between current collecting substrate and electrode material. The value of specific capacitance for C6 was higher than C1 and C4 electrodes which is attributed to its lower charge transfer resistance caused by a presence of two metal hydroxides.

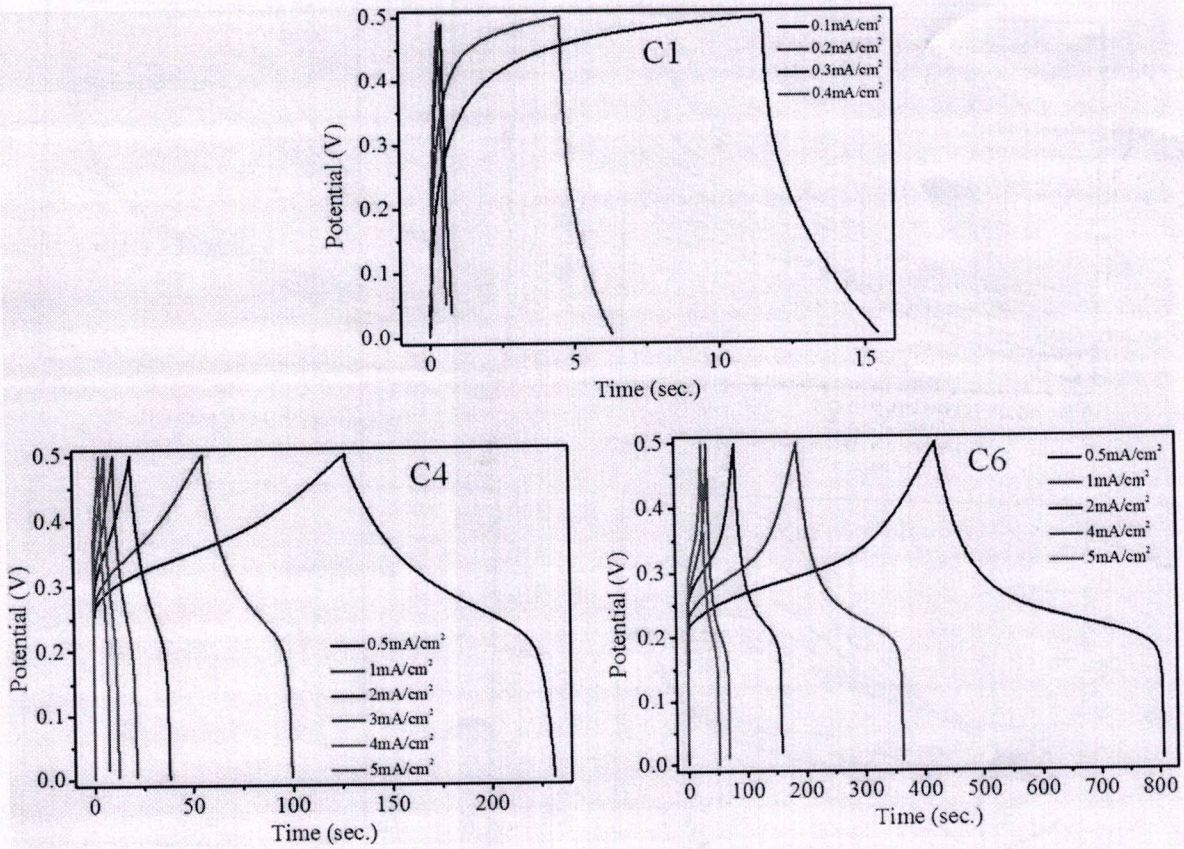

Fig. 8. The GCD measurements of C1, C4 and C6 electrodes.

Galvanostatic charge-discharge measurement

The specific capacitance (Cs), energy density (E) and power density (P) from GCD curves (Fig. 8) of C1–C6 electrodes were determined by following equations

$$C_s = \frac{It}{m\nabla V} \tag{12}$$

$$E = \left(\frac{1}{2}\right) C_s (\nabla V)^2 \tag{13}$$

$$P = \frac{E}{t} \tag{14}$$

where, I is the discharging current (mA) and t is the discharging time (s). The Cs values of C1, C4 and C6 electrodes calculated by GCD curves were respectively 0.28 F/g at 0.1 mA/cm^2, 37.07 F/g at 0.5 mA/cm^2 and 136.78 F/g at 0.5 mA/cm^2 as PANI (C1) shows a low charge induction capacity, due to which, the charge-discharge plot was attempted at lower current density value than other two electrodes. From the charge-discharge plots electrode C6 demonstrated better capacitive performance than both PANI and other NCs electrode materials due to its higher charging-discharging time within a fixed potential window.

Conclusions

This manuscript presents synthesis and studied on physical and electrochemical properties of PANI, PANI/$Co(OH)_2$–$Ni(OH)_2$ and $Co(OH)_2$–$Ni(OH)_2$ electrode materials onto a stainless-steel substrate. Elemental mapping analysis has, un-doubtedly, supported the synthesis of these electrode materials. All electrode materials have contributed an amorphous crystal structure however, there is significant change in their surface appearance i.e. from nanorods to platelets with an addition of $Co(OH)_2$-$Ni(OH)_2$. An electrochemical performance measurements attempted on these electrode materials confirm better energy storage potential in $Co(OH)_2$-$Ni(OH)_2$ over PANI and NCs electrode materials as its specific capacitance, energy density, power density measured from both CV and GCD measurements at 10 mV/s were much higher, suggesting the use of PANI with metal oxides/hydroxides is unable to produce synergic effect which we experience/expect in other composite electrodes materials.

References

[1] Kotz R, Muller S, Bartschi M, Schnyder B, Dietrich P, Buchi FN, et al. Supercapacitors for peak-power demand in fuel-cell-driven cars. Electrochem Soc Proc 2001;21:564–75.
[2] Fic K, Platek A, Piwek J, Frackowiak E. Sustainable materials for electrochemical capacitors. Mater Today 2018;21:437–54.
[3] Arencibia N, Oestreicher V, Viva FA, Jobbagy M. Nanotextured alpha Ni (II)–Co (II) hydroxides as supercapacitive active phases. RSC Adv 2017;7:5595–600.
[4] Wang G, Zhang L, Zhang J. A review of electrode materials for electrochemical supercapacitors. Chem Soc Rev 2012;41:797–828.
[5] Liu J, Zhang L, Wu HB, Lin J, Shen Z, Lou XW. High-performance flexible asymmetric supercapacitors based on a new graphene foam/carbon nanotube hybrid film. Energy Environ Sci 2014;7:3709–19.
[6] Wang H, Lin J, Shen ZX. Polyaniline (PANi) based electrode materials for energy storage and conversion. J Sci: Adv Mater Devices 2016;1:225–55.
[7] Wang F, Xiao S, Hou Y, Hu C, Liu L, Wu Y. Electrode materials for aqueous asymmetric supercapacitors. RSC Adv 2013;3:13059–84.
[8] Ramya R, Sivasubramanian R, Sangaranarayana MV. Conducting polymers-based electrochemical supercapacitors-progress and prospects. Electrochim Acta 2013;101(101):109–29.
[9] Naseri M, Fotouhi L, Ehsani A. Recent progress in the development of conducting polymer-based nanocomposites for electrochemical biosensors applications: a mini-review. Chem Rec 2018;18:599–618.
[10] Yang MH, Choi BG. High-performance asymmetric supercapacitors based on polyoxometalate-graphene nanohybrids. Carbon Lett 2016;18:84–9.
[11] Wang J, Zhang Y, Ye J, Wei H, Hao J, Mu J, et al. Facile synthesis of three-dimensional $NiCo_2O_4$ with different morphology for supercapacitors. RSC Adv 2016;6:70077–84.
[12] Kumar KS, Choudhary N, Jung Y, Thomas J. Recent advances in two-dimensional

nanomaterials for supercapacitor electrode applications. ACS Energy Lett 2018;3:482–95.
[13] Kim KH, Mikami M, Abe Y, Kawamura M, Kiba T. Structural and electrochemical properties of nanolayer-stacking structured copper-doped nickel hydroxide. Int J Electrochem Sci 2018;13:7655–62.
[14] Gao Y, Zhao J, Run Z, Zhang G, Pang H, Gao Y, et al. Microporous $Ni_{11}(HPO_3)_8(OH)_6$ nanocrystals for high-performance flexible asymmetric all solid-state supercapacitors. Dalton Trans 2014;43:17000–5.
[15] Ji Y, Liu W, Zhang Z, Wang Y, Zhao X, Li B, et al. Heterostructural MnO_2@NiS_2/Ni $(OH)_2$ materials for high-performance pseudocapacitor electrodes. RSC Adv 2017;7:44289–95.
[16] Wang X, Yan C, Sumboja A, Lee PS. High performance porous nickel cobalt oxide nanowires for asymmetric supercapacitor. Nano Energy 2014;3:119–26.
[17] Ge X, Gu CD, Wang XL, Tu JP. Ionothermal synthesis of cobalt iron layered double hydroxides (LDHs) with expanded interlayer spacing as advanced electrochemical materials. J Mater Chem A 2014;2:17066–76.
[18] Gu Y, Lu Z, Chang Z, Liu J, Li Y, Sun X. NiTi layered double hydroxide thin films for advanced pseudocapacitor electrodes. J Mater Chem A 2013;1:10655–61.
[19] Wang F, Wang T, Sun S, Xu Y, Yu R, Juan H. One-step synthesis of Nickle Iron-layered double hydroxide/reduced graphene oxide/carbon nanofibres composite as electrode materials for asymmetric supercapacitor. Sci Rep 2018;8:8908–18.
[20] Li L, Qin J, Bi H, Gai S, He F, Gao P, et al. Ni $(OH)_2$ nanosheets grown on porous hybrid g-C_3N_4/RGO network as high performance supercapacitor electrode. Sci Rep 2017;7:43413–24.
[21] Dong B, Li M, Chen S, Ding D, Wei W, Gao G, et al. Formation of g-C_3N_4@ Ni $(OH)_2$ honeycomb nanostructure and asymmetric supercapacitor with high energy and power density. ACS Appl Mater Interfaces 2017;9:17890–6.
[22] Zhu ZY. Electrochemical properties of Ni $(OH)_2$/MnO_2 on hybrid N-doped carbon structure as high-performance electrode material. AIP Adv 2018;8:075223–32.
[23] Adhikari AD, Oraon R, Tiwari SK, Jena NK, Lee JH, Kim NH, et al. Polyaniline-stabilized intertwined network-like ferrocene/graphene nanoarchitecture for supercapacitor application. Chem Asian J 2017;12:900–9.
[24] Jin L, Jiang Y, Zhang M, Li H, Xiao L, Li M, et al. Oriented polyaniline nanowire arrays grown on dendrimer (PAMAM) functionalized multiwalled carbon nanotubes as supercapacitor electrode materials. Sci Rep 2018;8:6268–78.
[25] Qorbani M, Naseri N, Moshfegh AZ. Hierarchical Co_3O_4/$Co(OH)_2$ nanoflakes as a supercapacitor electrode: experimental and semi-empirical model. ACS Appl Mater Interfaces 2015;7:11172–9.
[26] Shi P, Chen R, Li L, An J, Hua L, Zhou J, et al. Holey nickel hydroxide nanosheets for wearable solid-state fiber-supercapacitors. Nanoscale 2018;10:5442–8.
[27] Xu T, Li G, Zhao L. Ni-Co-S/Co $(OH)_2$ nanocomposite for high energy density all-solid-state asymmetric supercapacitors. Chem Eng J 2018;336:602–11.
[28] Brisse A, Stevens P, Toussaint G, Crosnier O, Brousse T. Ni $(OH)_2$ and NiO based composites: battery type electrode materials for hybrid supercapacitor devices. Materials 2018;11:1178–93.
[29] Zhou H, Zhang L, Zhang D, Chen S, Coxon PR, He X, et al. A universal synthetic route to carbon nanotube/transition metal oxide nano-composites for lithium ion batteries and electrochemical capacitors. Sci Rep 2016;6:37752–63.
[30] Devarayan K, Lei D, Kim HY, Kim BS. Flexible transparent electrode based on PANi nanowire/nylon nanofiber reinforced cellulose acetate thin film as supercapacitor. Chem Eng J 2015;273:603–9.